NANO LETTERS
2007
Vol. 7, No. 11
3320−3323

Photocurrent Imaging of p–n Junctions in Ambipolar Carbon Nanotube Transistors

Y. H. Ahn,[†] A. W. Tsen,[‡] Bio Kim,[§] Yung Woo Park,[§] and Jiwoong Park*[,‡,#]

Division of Energy Systems Research, Ajou University, Suwon 443-749, Korea, Department of Chemistry and Chemical Biology, Cornell University, Ithaca, New York 14853, Department of Physics and Astronomy, Seoul National University, Seoul 151-742, Korea, and The Rowland Institute at Harvard, Harvard University, Cambridge, Massachusetts 02142

Received June 27, 2007; Revised Manuscript Received August 22, 2007

ABSTRACT

We use scanning photocurrent microscopy (SPCM) to investigate the properties of internal p–n junctions in ambipolar carbon nanotube (CNT) transistors. Our SPCM images show strong signals near metal contacts whose polarity and positions change depending on the gate bias. SPCM images analyzed in conjunction with the overall conductance also indicate the existence and gate-dependent evolution of internal p–n junctions near contacts in the n-type operation regime. To determine the p–n junction position and the depletion width with a nanometer scale resolution, a Gaussian fit was used. We also measure the electric potential profile of partially suspended CNT devices at different gate biases, which shows that induced local fields can be imaged using the SPCM technique. Our experiment clearly demonstrates that SPCM is a valuable tool for imaging and optimizing electrical and optoelectronic properties of CNT based devices.

In semiconducting nanostructures, including carbon nanotubes (CNTs)[1,2] and nanowires (NWs),[3] the electronic properties at various interfaces, especially metal contacts, play a crucial role, often dominating the overall performance of nanostructure-based devices.[4−7] In addition, the presence and properties of defects can cause various abnormalities in the conductance properties. To fully understand the overall conductance behavior of a nanostructure with high spatial resolution, various scanning probe microscopy (SPM) techniques have been utilized to locally perturb or electrically contact the target structures.[7,8]

More recently, scanning photocurrent microscopy (SPCM) has been successfully applied to study electrical and photoelectric properties of a number of linear nanostructures, including carbon nanotubes[9−11] and semiconducting nanowires.[12,13] The information generated by SPCM includes the band structure near nanostructure/metal interfaces,[11,13] carrier relaxation dynamics,[14] and detection of local defects.[10]

In this paper, we report SPCM measurements of CNT transistors at different gate biases (V_G's) to investigate the electronic band structure. Our measurements reveal that the peak photocurrent (PC) spots near the metal contacts move with gate bias in the n-type regime. We measure with nanoscale resolution the intensity and polarity of these PC spots in conjunction with DC conductance to investigate the dynamics of the internal p−n junctions. We also study the effect of various local potential variations such as induced electrical field due to a partial suspension of the CNTs.

Our CNT transistors were fabricated using standard photolithography and electron beam lithography techniques with CVD-grown semiconducting CNTs. CNTs were first synthesized directly on a 220 nm thick thermal oxide layer on a conducting Si substrate that is also used as a back gate. Metal evaporation and liftoff were used to define drain and source electrodes. We used either Cr/Au (5/45 nm) or Ti (50 nm) for the electrodes.

Our SPCM setup uses a diffraction-limited laser beam scanned over the CNT devices, and the photocurrent is recorded as a function of the position of the laser spot.[13] We also monitor the reflected light intensity simultaneously to determine the absolute position of the laser spot. The schematic of the setup is shown in Figure 1a. To improve the performance we used a lock-in technique with an intensity-modulated laser (λ = 781 nm with 20 kHz modulation, unless otherwise noted). The signal-to-noise ratio is dramatically improved this way and we can reliably detect a low-level current signal (<10 pA) measured with a low light intensity.

* Corresponding author. E-mail: jp275@cornell.edu.
† Ajou University.
‡ Cornell University.
§ Seoul National University.
# Harvard University.

10.1021/nl071536m CCC: $37.00 © 2007 American Chemical Society
Published on Web 10/16/2007

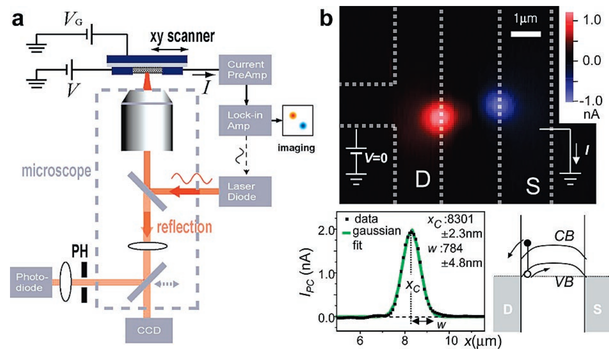

Figure 1. (a) Schematic of the SPCM setup. (b) SPCM image of a semiconducting CNT device **D1**. Left inset: Gaussian fit to one of the PC spots for determining the peak position and width. Right inset: mechanism of the contact PC generation.

In Figure 1b, we show a representative SPCM image taken at $V_G = V_{SD} = 0$ with a device **D1** fabricated with a semiconducting CNT. It clearly shows localized PC spots near both electrode contacts. These localized PC spots are due to electronic band bending (or equivalently, a local electric field) near the metal/CNT interfaces.[12,13] Here, the polarity of the PC indicates that the electronic band bends upward toward the middle of the CNT (see the second inset of Figure 1b). Similar photocurrent features were observed from most semiconducting CNT devices measured to date (more than 20 devices), but their magnitude (typically of the order of 1 nA for the light intensity of 100 kW/cm^2) varies from device to device.

Because the zero-bias PC signal originates from local electric fields, the position, intensity, and shape of the PC signals provide detailed information about the local electric potential in CNT devices. Furthermore, the peak position and extent of local fields can be determined from the measured PC signal with nanometer-scale resolution (much smaller than the focused laser spot) using a 1D or 2D Gaussian fit method. An example of a 1D Gaussian fit to our PC data is shown in the inset to Figure 1b.

Below we first discuss the properties of the contact PC spots measured as a function of V_G to investigate CNT electron band structure for both p- and n-type operation. To this end, we limit our discussion to CNTs with a relatively small band gap, the regime where we can clearly observe both p- and n-type operation.

The upper images in Figure 2a,b each show a spatial SPCM image of devices **D2** and **D3** measured at a negative V_G. The lower images show the gate-dependent behavior of the contact PC spots, measured along the dashed line in the upper image, V_G being swept from -2.5 V to a positive value (3.5 V in 2a and 2.5 V in 2b). **D2** and **D3** are contacted by Cr/Au and Ti, respectively. The CNTs in both devices are semiconducting with a relatively small band gap (estimated to be less than 0.3 eV from the conductance measurements). In both devices, the PC spots near the contacts change polarity at a certain gate bias, $V_{G;FB}$. We also note that in both devices the polarity changes continuously from positive to negative (negative to positive) near the drain (source) electrode as V_G is swept in the positive direction.

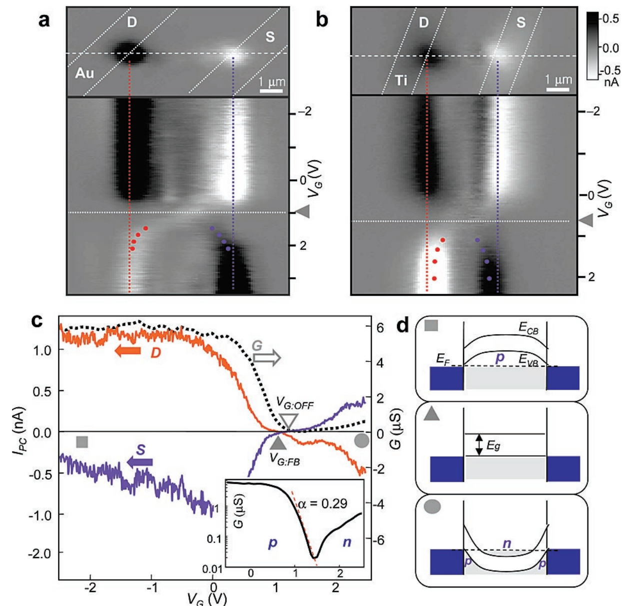

Figure 2. Gate bias dependence of PC for a semiconducting CNT device **D2** (a) and **D3** (b). (c) PC measured at source (S) and drain (D) electrodes and dc conductance (G) are shown. Inset: semilogarithmic plot of G vs V_G. (d) Band structures for p-type (■), flat band (▲), and n-type (●) cases.

The behaviors discussed above are due to the direction change of the electronic band bending at the contact. As V_G increases, the electron band of the middle portion of the CNT moves downward, whereas it is pinned at the contact. As a result, the band-bending direction changes at higher V_G. Here the critical gate bias at which the PC polarity flips (zero PC) signifies the configuration where the electron band is flat near either contact (flat band; $V_{G;FB}$). In Figure 2a,b, $V_{G;FB}$ is approximately 1.0 and 0.7 V, respectively, and it is denoted by a solid triangle with a dotted line.

Comparison with the simultaneously measured DC conductance illuminates quantitative details regarding the electron band alignment at the contact. In Figure 2c, we show the PC near the drain (D) and source (S) electrodes as well as the linear conductance (G) as a function of V_G measured from **D2**. Titanium contacted **D3** shows a similar behavior (not shown). The polarity of both PC signals changes around $V_{G;FB} \sim 1.0$ V (denoted by a solid triangle), and the conductance reduces to nearly zero at $V_{G;OFF} \sim 1.1$ V (open triangle). The conductance then increases when $V_G > 1.5$ V as the CNT device becomes n-type (see inset, Figure 2c). In **D3**, $V_{G;FB}$ and $V_{G;OFF}$ is measured closer to each other than in **D2**. In both devices, the energy difference, $\Delta = |E_{VB} - E_F|$, between the valence band and the Fermi level can be estimated using $\Delta = \alpha|e(V_{G;FB} - V_{G;OFF})|$ where α is the gate efficiency and e is the electron charge. Using the procedure described earlier,[13,15] we find $\alpha = 0.29$ for **D2** (see inset, Figure 2c), and hence $\Delta \sim 30$ meV $\sim k_BT$ (k_B: Boltzmann constant). We measure $|\Delta| < 10$ meV for **D3**. Assuming that the conductance shut-off at $V_{G;OFF}$ occurs when the edge of the valence band is aligned with the Fermi level, this indicates that the CNT valence bands in both **D2**

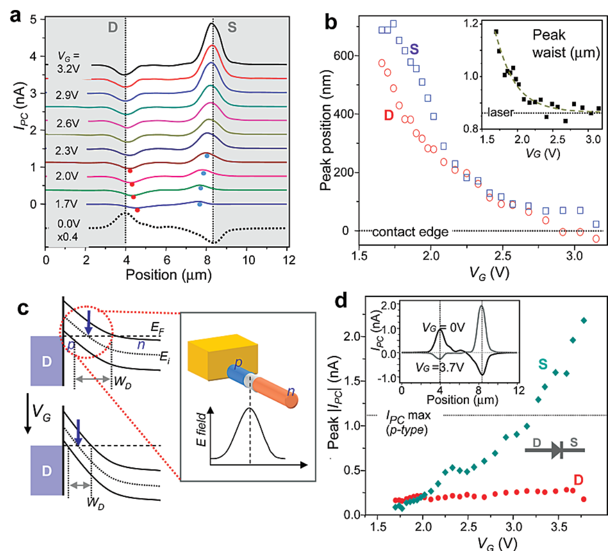

Figure 3. Internal p−n junction in an n-type CNT. (a) PC line scans from **D2** in the n-type regime. (b) PC peak position vs V_G obtained using the Gaussian fit method. Inset: peak waist (drain side) vs V_G. (c) A p−n junction and depletion region (W_D) at different V_G's. (d) PC enhancement (source side) and suppression (drain side) in the n-type CNT device.

and **D3** are closely aligned to the Fermi level within the thermal excitation energy at the contacts.[16]

The data shown in Figure 2 together with the discussion given above provide strong evidence that the contact region of the CNT in both **D2** and **D3** is p-type. In addition, we expect a large density of holes at the contact in both devices based on the band alignment discussed above. In Figure 2d, the electron band alignment near the contacts in the p-type (■), flat band (▲), and n-type (●) cases are depicted.

Significantly, in the n-type regime there should exist internal p−n junctions near the electrodes, as only the main body of the CNT turns n-type. The presence of internal p−n junctions in CNT devices will have a strong impact on both the conductance and PC behaviors. In particular, a strong local electric field is expected at the p−n junction, with its maximum located at the center of the depletion region. Therefore, the maximum PC will coincide with the position of the p−n junction. Indeed we observe several distinctive properties of PC signals in the n-type regime that are consistent with this model, as described below.

In Figure 3a, we show the line scans of PC measured from **D2** in the n-type regime at various V_G's. The most striking feature in this plot is the movement of contact PC spots as V_G changes. The PC peaks move away from the contact region (shaded area) and approach the middle of the CNT as V_G decreases. On the contrary, the PC spots in the p-type regime do not change throughout the whole gate bias range.

In Figure 3b, we measure the PC peak positions and widths as a function of V_G using the Gaussian fit method described in Figure 1b, which shows the PC peak movement with the same trend as described above. Surprisingly, the PC peak moves more than 0.6 μm away from the contact, beyond which the PC signal is too weak for a precise measurement. In addition, the Gaussian fit width (inset, Figure 3b) measured from the PC spot indicates an increasing peak width as V_G decreases. Similar gate dependent behaviors were observed in most semiconducting devices studied to date, including **D3**.

We can understand these behaviors in terms of the internal p−n junctions in n-type operation discussed earlier, as shown in Figure 3c. As V_G increases, the main body of the CNT becomes n-type when E_i (intrinsic level of the CNT) becomes lower than E_F. Because the contact region is still p-type, a large portion of the CNT will form a depletion region. As V_G increases further, the position of the depletion region (W_D) and the p−n junction will move closer to the contact while the width of W_D becomes narrower. The electric field and the potential around the p−n junction are analogous to the case of a linearly varying dopant in conventional semiconductor p−n junctions. In this model, the electric field is at a maximum in the middle of the W_D and is strong over the extent of W_D.[17]

Although the presence of internal p−n junctions is also supported by the conductance measurement (this can be seen from the inset to Figure 2c, where the conductance increases exponentially with increasing V_G in the deep n-type regime), our data presented in Figure 3 provide a direct measure of the evolution of the p−n junctions in much greater spatial detail. Interestingly, we note that the p−n junction can stay away from the contact even deep into the n-type region, as can be seen for **D3** in Figure 2b (red and blue dots). There, the PC spots stay approximately 200 nm away from the contact throughout most of the n-type regime. Previously, low-temperature conductance measurements on similar devices reported the formation of a p-type quantum dot (size ∼ 100 nm) near the contact whereas the main body of the CNT is n-type.[18] Our experiment provides the first photoelectric measurements on such p−n junctions with nanoscale spatial resolution.

One of the useful properties of a p−n junction is its high efficiency for electron−hole separation and thus sensitive photoresponse. We often observe that the n-type PC signal is indeed strongly enhanced compared to the p-type case, as demonstrated in Figure 3d. Although the magnitude of p-type PC in this device always stays below 1.1 nA, for both electrodes, the n-type PC near the source contact keeps increasing above 2.3 nA with no saturation. On the contrary, the n-type PC is strongly suppressed for the drain electrode. These behaviors can be explained if the device has a larger p−n junction resistance near the source electrode than near the drain electrode. In that case, the strong electric field at each p−n junction will push light-excited holes to nearby electrodes, whereas the light-excited electrons are collected predominantly by the drain electrode because of the lower resistance. As a result, these PC behaviors in the n-type regime make the entire CNT device equivalent to a single sensitive p−n junction photodiode.

Because SPCM produces local information regarding the electric field in CNT devices, it can be used to detect and map out potential variations in the device. In Figure 4, we demonstrate the use of SPCM to map out the electric potential profile in a partially suspended CNT device, **D4**.

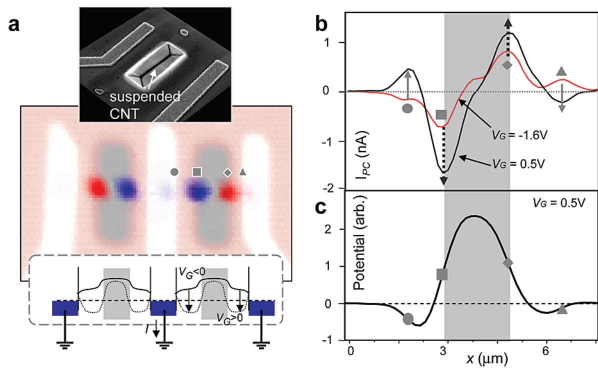

Figure 4. Electric potential profile in a partially suspended CNT device. (a) An SEM and SPCM image from a suspended CNT device, **D4**. Gray areas denote suspended parts. Inset: expected band movement for different V_G's. (b) PC measured at $V_G = -1.6$ and 0.5 V. (c) Electron energy profile obtained by integrating PC shown in (b).

Even though this device geometry has attracted wide attention for both nanoelectromechanical systems[19] and high efficiency light emitters,[20] understanding the strength of local electric fields in this device geometry has been difficult due to the limitations of SPM techniques. In Figure 4a, we show both an electron micrograph and a combined SPCM/reflected light image measured on **D4** ($V_G = 0$ V). In this device, a single CNT is contacted by three electrodes, and the middle electrode was used to capture the PC. Strong PC spots are clearly observed at the edges of suspended parts of the CNT, which indicate that the electric field is strong there. This is consistent with the mechanism given for the highly efficient electroluminescenece measured in partially suspended CNT devices.[20] In addition, the polarity of these PC signals indicates that the electron band is higher in the suspended part compared to the supported part (see the inset).[21] The absence of a PC signal near the contacts indicates that the band is flat there.

When we change V_G, it is expected that the electron band in the supported parts moves more closely with V_G due to the larger dielectric constant of the substrate ($\epsilon_{SiO_x} = 3.8$) compared to air. Indeed this is the case as shown in the line scans taken at different V_G's. If we first decrease V_G to -1.6 V, the band of the supported parts move upward to produce significant contact PC signals. As we increase V_G from negative to positive (0.5 V), the electron band of the supported parts moves downward much faster than in the suspended parts. As a result, the PC at the edges of the suspended parts becomes much stronger due to a larger energy difference between adjacent CNT portions and the correspondingly stronger electric field that exists at these locations. In addition, the contact PC changes its polarity at a positive V_G. In Figure 4c, we plot the electron band obtained by integrating the PC curve for $V_G = 0.5$ V, which closely matches the expected band movement shown in the inset to Figure 4a.

In conclusion, the SPCM is a powerful tool for understanding the electron band structure in CNT-based devices. It can produce detailed information regarding the properties of internal p−n junctions and induced electric fields. Furthermore, the resulting photoelectric information in diverse device configurations with nanoscale spatial resolution will serve as an important guideline for optimizing and interrogating the underlying mechanisms in CNT based electrical, optoelectronic and photovoltaic devices.

Acknowledgment. We thank M. Burns for helpful discussions. This work was mainly supported by the Rowland Junior Fellow program. Y.H.A. is also supported by the Nanoscopia Center of Excellence at Ajou University. B.K. was partially supported by the BK21 Frontier Physics Research Division of Seoul National University.

References

(1) McEuen, P. L.; Park, J. Y. *MRS Bull.* **2004**, *29*, 272−275.
(2) Avouris, P. *MRS Bull.* **2004**, *29*, 403−410.
(3) Lieber, C. M. *MRS Bull.* **2003**, *28*, 486−491.
(4) Heinze, S.; Tersoff, J.; Martel, R.; Derycke, V.; Appenzeller, J.; Avouris, P. *Phys. Rev. Lett.* **2002**, *89*, 106801.
(5) Appenzeller, J.; Knoch, J.; Derycke, V.; Martel, R.; Wind, S.; Avouris, P. *Phys. Rev. Lett.* **2002**, *89*, 126801.
(6) Javey, A.; Guo, J.; Paulsson, M.; Wang, Q.; Mann, D.; Lundstrom, M.; Dai, H. J. *Phys. Rev. Lett.* **2004**, *92*, 106804.
(7) Yaish, Y.; Park, J. Y.; Rosenblatt, S.; Sazonova, V.; Brink, M.; McEuen, P. L. *Phys. Rev. Lett.* **2004**, *92*, 046401.
(8) Bachtold, A.; Fuhrer, M. S.; Plyasunov, S.; Forero, M.; Anderson, E. H.; Zettl, A.; McEuen, P. L. *Phys. Rev. Lett.* **2000**, *84*, 6082−6085.
(9) Balasubramanian, K.; Fan, Y. W.; Burghard, M.; Kern, K.; Friedrich, M.; Wannek, U.; Mews, A. *Appl. Phys. Lett.* **2004**, *84*, 2400−2402.
(10) Balasubramanian, K.; Burghard, M.; Kern, K.; Scolari, M.; Mews, A. *Nano Lett.* **2005**, *5*, 507−510.
(11) Freitag, M.; Tsang, J. C.; Bol, A.; Yuan, D.; Liu, J.; Avouris, P. *Nano Lett.* **2007**, *7*, 2037−2042.
(12) Gu, Y.; Kwak, E.-S.; Lensch, J. L.; Allen, J. E.; Odom, T. W.; Lauhon, L. J. *Appl. Phys. Lett.* **2005**, *87*, 043111.
(13) Ahn, Y.; J., D.; Park, J. *Nano Lett.* **2005**, *5*, 1367−1370.
(14) Gu, Y.; Romankiewicz, J. P.; David, J. K.; Lensch, J. L.; Lauhon, L. J. *Nano Lett.* **2006**, *6*, 948−952.
(15) Rosenblatt, S.; Yaish, Y.; Park, J.; Gore, J.; Sazonova, V.; McEuen, P. L. *Nano Lett.* **2002**, *2*, 869−872.
(16) Quantitative details of the band alignment parameters discussed here will change for different CNT devices, depending on various conditions such as the bandgap of CNT, the metal work function, and/or the electrostatic environment near the contacts. Our SPCM technique will allow a systematic study on the effect of these conditions on the band parameters, which is outside the scope of this paper.
(17) Sze, S. M. *Physics of Semiconductor Devices*; John Wiley & Sons: New York, 1981; Vol. 2.
(18) Park, J.; McEuen, P. L. *Appl. Phys. Lett.* **2001**, *79*, 1363−1365.
(19) Sazonova, V.; Yaish, Y.; Ustunel, H.; Roundy, D.; Arias, T. A.; McEuen, P. L. *Nature* **2004**, *431*, 284−287.
(20) Chen, J.; Perebeinos, V.; Freitag, M.; Tsang, J.; Fu, Q.; Liu, J.; Avouris, P. *Science* **2005**, *310*, 1171−1174.
(21) All of our partially suspended CNT devices we tested show the relative p-doping in the suspended part of CNTs. This is likely due to the acid (HF) treatment that only the suspended part was exposed to during the fabrication of the trench. Even though the effect of HF on the CNT properties has not been investigated, a strong acid such as a nitric acid is routinely used for the oxidation of CNTs.

NL071536M